# Fully nonlinear dynamics of parallel wakes

### By JEAN-MARC CHOMAZ

LadHyX, CNRS–Ecole Polytechnique, 91128 Palaiseau, France

The fully nonlinear theory of global modes in open flows, proposed in recent analyses of amplitude equations, is extended to the case of Navier–Stokes equations using direct numerical simulations. The basic flow under consideration is a parallel wake in a finite domain generated by imposing the wake profile at the inlet boundary and by adding a body force to compensate the basic flow diffusion. The link between the global bifurcation, the absolute or convective nature of the local linear instability, and the theory of speed selection for the front separating an unperturbed domain of the flow from a fully saturated solution is elucidated. In particular, thanks to the parallelism of the flow, the bifurcation scenario and the associated scaling laws for the frequency, the healing length, and the slope at the origin predicted by a previous analysis of amplitude equations are recovered with great precision.

## 1. Introduction

Open flow behaviour was elucidated in the 1980s thanks to the concept of convective and absolute instabilities that differentiates flows for which perturbations are amplified but advected downstream from those for which perturbations are amplified strongly enough to sustain the mean advection (see Huerre & Monkewitz 1990). This theory has been able to predict the occurrence of self-sustained resonances in counter-flow mixing layers (Strykowski & Niccum 1991), hot or helium jets (Sreenivasan, Raghu & Kyle 1989; Monkewitz *et al.* 1990; Kyle & Sreenivasan 1993; Yu & Monkewitz 1993), wakes with or without suction (Hammond & Redekopp 1997; Woodley & Peake 1997), and rotating disks (Lingwood 1995, 1996). Despite these successes there remains a mist of mystery, since nonlinear effects do not modify the instability threshold nor the oscillation frequency predicted by the linear absolute instability theory as expected from the already strong instability of the flow when self-sustained oscillations occur. For example, variable-density jets or mixing layers with counter-flow exhibit a noise amplifier behaviour, prior to the resonance, and low-level inlet perturbations, unavoidable in experiments, lead to fully developed instabilities under the threshold of the self-sustained oscillations. Similarly, a small perturbation of a cylinder wake at a Reynolds number of 40, smaller than the critical Reynolds number of 47 above which oscillations are self-sustained, has been shown to give rise to a strong amplified transient where nonlinear saturation has already occurred (Delbende & Chomaz 1998). Recently, by considering model equations describing the amplitude of instability waves, two teams have succeeded in solving this apparent paradox for the occurrence of a strongly nonlinear self-sustained oscillation predicted by a linear criterion. The basic ideas were proposed in Chomaz (1992) where a nonlinear extension of the concept of absolute and convective instability was introduced as illustrated on figure 1: "The basic state of a system is *nonlinearly stable* if for all initial perturbations of finite extent and amplitude, the system relaxes to the basic
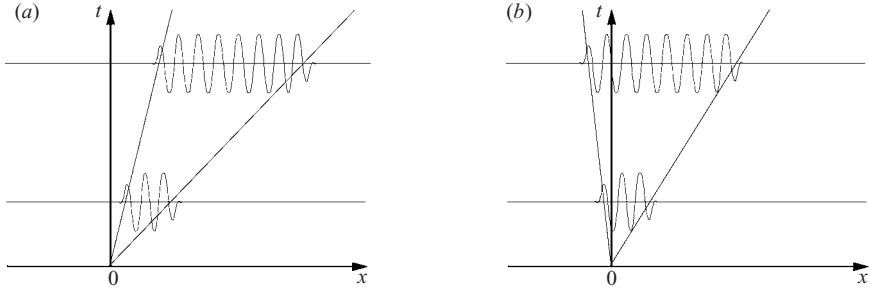
FIGURE 1. Diagrams in the $(x, t)$-plane, displaying the dynamics of a saturated wave packet in a linearly unstable flow issuing from an initial localized perturbation: (*a*) nonlinear convective instability, the velocity $v_f$ of the trailing front separating the saturated wave from the basic state is positive; (*b*) nonlinear absolute instability, the front velocity $v_f$ is negative.

state everywhere in any moving frame. The system is unstable if it is not stable in the above sense. The instability is *nonlinearly convective* if, for all initial perturbations of finite extent and finite amplitude, the system relaxes to the basic state everywhere in the laboratory frame. It is *nonlinearly absolute* if, for some initial condition of finite extent and amplitude, the system does not relax to the basic state everywhere in the laboratory frame." In the above definition, the 'laboratory frame' refers to an experimental situation and is used to describe the frame specified by boundary conditions, inhomogeneities of the flow, forcing, etc.

The link between the linear criterion for the transition from convective to absolute instability, based on the impulse response, and its nonlinear counterpart may be established by referring to the work of Kolmogorov, Petrovsky & Piskunov (1937), Dee & Langer (1983), Dee (1985), Ben-Jacob *et al.* (1985), van Saarloos (1987, 1988, 1989), Powell, Newell & Jones (1991) and van Saarloos & Hohenberg (1992) on amplitude equations. A front separating the basic state from a bifurcated saturated solution moves either at the speed of the edge of the linear wave packet generated by the linear impulse response, as observed by Dee & Langer (1983), or faster if a nonlinear marginal stability condition is fulfilled (van Saarloos & Hohenberg 1992). When the front moves at the linearly determined velocity of the edge of the wave packet, it is called a pulled front since the dynamics is governed by the instability properties upstream of the front where linear theory is valid. As shown by Chomaz & Couairon (2000), the fast nonlinear solution is in fact selected by causality and is referred to as the pushed front, since the saturated region drives the dynamics, and forces the linear region upstream of the front, in contrast to the pulled front. The result that a front moves at the same speed or faster than the pulled front implies that the linear absolute instability is only a sufficient condition for a nonlinear absolute instability (see Couairon & Chomaz 1996, 1997*b* for details).

When the front is pulled, linear absolute instability and nonlinear absolute instability coincide. In this case Couairon & Chomaz (1996, 1997*a*, *b*, 1999*b*) have shown that, in a semi-infinite domain with vanishing inlet perturbations, a self-sustained oscillation (a so-called global mode) occurs as soon as the instability is absolute. At the threshold, the selected frequency is the absolute frequency. As the control parameter is increased from the critical value at which the instability becomes absolute, the self-sustained oscillation saturates closer to the inlet and is described at leading order by a front blocked by the inlet condition. This front would have moved upstream in the absence of the boundary condition. Similar results were numerically

obtained in parallel by Meunier *et al.* (1997) and Tobias, Proctor & Knobloch (1997, 1998) for the particular case of the supercritical Ginzburg–Landau equation and by Worledge *et al.* (1997) for the Parker dynamo equations. In this case, Couairon & Chomaz (1997*a*,*b*, 1999*b*) have shown that the so-called 'healing length' defined as the distance at which saturation occurs, scales as the inverse of the square root of the criticality (the difference between the actual control parameter and its critical value). This bifurcation scenario and the corresponding frequency selection criteria and scaling laws have been verified by numerical simulations of amplitude equations (Couairon & Chomaz 1996, 1997*a*,*b*, 1998). This theory also properly describes the behaviour of two open flows generated by adding a throughflow to the Rayleigh–Bénard convection (Fineberg & Steinberg 1987 and Müller, Lücke & Kamps 1989, 1992) and to the Taylor–Couette experiments (Ahlers & Cannel 1983 and Büchel *et al.* 1996).

By comparing numerical simulations of the linear impulse response for a parallel wake with their nonlinear counterparts, Delbende & Chomaz (1998) have shown that the front separating the von Kármán saturated street from the unperturbed stationary wake moves at a constant speed equal to that of a pulled front. This important numerical demonstration that the nonlinear wake instability follows the Dee & Langer (1983) scenario explains why the linear theory for convective and absolute instabilities has been successful when describing the wake bifurcation. Recently, Pier & Huerre (2001) used this result to show that a decelerating pressure gradient was able to destabilize a wake velocity profile and Pier (2002) compared the frequency selection of the vortex shedding in the cylinder wake with that obtained from the theory for convective and absolute instabilities. In these cases, the flow is non-parallel and the resulting global mode includes a front located at the streamwise location where its velocity vanishes, i.e. at the convective/absolute transition location since the pulled front is selected according to the linear marginal stability criterion. Similar results on the effect of the non-parallelism of the flow have been derived previously for model amplitude equations with variable coefficients by Harris, Bassom & Soward (2000) and Soward (2003).

The present paper goes one step further and demonstrates that the bifurcation scenario, the selection principle and the scaling laws rigorously established in the context of generalized Ginzburg–Landau equations do apply to wake flows. In order to do so in an extremely precise way, the evolution of a wake in a finite rectangular domain is numerically computed. The wake profile is directly imposed at the inlet location. Indeed, as already demonstrated by Triantafyllou & Karniadakis (1990) the wake flow is identical if the cylinder region is cut off and replaced by an inlet condition on a line normal to the mean flow axis instead of computing the dynamics of the whole flow around a cylinder. To further validate the theoretical predictions, the extra complexity of the non-parallelism of the flow has been avoided by adding an artificial body force that exactly compensates the diffusion of the basic flow. This method is systematically used to analyse the linear instability of viscous shear flows (cf. Drazin & Reid 1981). When the non-parallelism of the real flow is weak enough, i.e. when the scale on which the basic flow varies is large enough compared to the typical length scale of the instability (the wavelength and/or the inverse of the spatial growth rate), the present results may be extended in a straightforward manner as discussed by Couairon (1997), Worledge *et al.* (1997), Couairon & Chomaz (1999*a*, 2001), Harris *et al.* (2000), Soward (2003), and Pier, Huerre & Chomaz (2001) for amplitude equations and by Pier & Huerre (2001) for a non-parallel synthetic wake flow in an infinite domain.

Although the parallel wake flow may seem artificial, it allows comparison with theory without approximations. It demonstrates the importance of nonlinear effects and the resulting non-standard bifurcation scenario. Even if weak non-parallel effects were present the classical Hopf bifurcation scenario would be valid for a very small criticality and the scenario illustrated in the present contribution would take over at larger values of the criticality as explained in Couairon & Chomaz (1999*a*) for model equations. The resulting discussion would have been more complicated, however, and the demonstration would have been limited to leading-order predictions as in Pier & Huerre (2001).

Therefore non-parallel effects are saved for a forthcoming publication and the present paper will only discuss the strong nonlinearities present in open flows when self-sustained oscillations occur. A new point of view based on saturated front dynamics is proposed, which allows a quantitative prediction of the behaviour of open flows. The next section presents the numerical procedures and the chosen basic flow. Comparison of the linear and nonlinear impulse responses is made in the following section. The dynamics of the wake flow in a semi-infinite box is presented in §4 and compared to theoretical predictions. Extensions of this work are proposed as a conclusion.

## 2. The numerical procedure

The numerical procedure is similar to that used in Delbende & Chomaz (1998). It integrates the two-dimensional Navier–Stokes equations perturbed around a basic flow with a velocity $\boldsymbol{U}_B = U_B(y)\boldsymbol{e}_x$ parallel to the $x$-direction only. The viscous dissipation of the basic flow $\boldsymbol{U}_B$ is compensated exactly by a body force $-\nu\Delta\boldsymbol{U}_B$. Experimentally such a forcing may be achieved in magnetohydrodynamic flows as in Bühler (1996). Let $\Omega_B = -\mathrm{d}U_B/\mathrm{d}y$ be the basic flow vorticity, $\boldsymbol{u} = u\boldsymbol{e}_x + v\boldsymbol{e}_y$ the perturbation velocity, $\omega\boldsymbol{e}_z = \nabla \times \boldsymbol{u}$ the perturbation vorticity, and $\phi$ the stream function such that $u = \partial\phi/\partial y$ and $v = -\partial\phi/\partial x$. The perturbed Navier–Stokes equations are

$$\left.\begin{aligned}
\frac{\partial\omega}{\partial t} &= J(\phi,\omega) - U_B\frac{\partial\omega}{\partial x} + \frac{\partial\phi}{\partial x}\frac{\partial\Omega_B}{\partial y} + \nu\Delta\omega, \\
\omega &= -\Delta\phi, \\
J(\phi,\omega) &= \frac{\partial\phi}{\partial x}\frac{\partial\omega}{\partial y} - \frac{\partial\omega}{\partial x}\frac{\partial\phi}{\partial y}.
\end{aligned}\right\} \tag{2.1}$$

The equations are integrated in a very long box of size $2L \times H$, periodic in the $x$-direction and with free-slip boundary conditions in the $y$-direction. As discussed in detail in Vincent & Meneguzzi (1991) the viscous term is integrated exactly in the spectral domain whereas other terms are estimated by a pseudo-spectral method and integrated in time using a leapfrog scheme with an Euler step every 320 time steps. The working time step is $5 \times 10^{-3}$ and the distance between collocation points is $\delta x = \delta y = 0.1$. Systematic convergence tests have been performed by varying the time step and the spatial resolution by factor 2 or 4 as explained in Billant, Brancher & Chomaz (1999). The effect of the temporal integration scheme has also been tested by verifying that the use of a second-order Adams–Bashforth scheme taken from Delbende, Chomaz & Huerre (1998) has no significant impact on the results.

We have chosen the basic wake profile elaborated by Monkewitz & Nguyen (1987):

$$U_B(y) = 2 + U_0 - \frac{2}{1 + \sinh^{2N}|y\sinh^{-1}(1)|}, \tag{2.2}$$

where $U_0$ is the centreline velocity, $U_\infty = 2 + U_0$ is the velocity at $y = \infty$, and $N$ is the parameter that controls the steepness of the shear layer. To compare with the results of Monkewitz & Nguyen (1987), we introduce the velocity ratio $\Lambda = (U_0 - U_\infty)/(U_0 + U_\infty) = -(1 + U_0)^{-1}$. This velocity profile has also been studied by Delfs *et al.* (1997) who have computed the linear impulse response and by Delbende & Chomaz (1998) who have compared the linear and the nonlinear impulse response. Both studies have shown the ability of direct numerical simulations to compute the absolute/convective transition of open flows (see also Delbende *et al.* 1998, for an application of the same technique to three-dimensional flows). In particular Delbende & Chomaz (1998) have computed the absolute instability transition as a function of $\Lambda$ and $N$ and, by means of numerical simulations of the impulse response, have recovered precisely the results of Monkewitz (1988) from the linear stability theory.

For all the simulations presented here, the initial perturbation corresponds to a vorticity dipole parallel to the $x$-axis with a Gaussian envelope:

$$\omega(t = 0) = \sin\left(\frac{y - y_0}{\delta}\right) \exp\left(\frac{(x - x_0)^2 + (y - y_0)^2}{\delta^2}\right), \tag{2.3}$$

with $(x_0, y_0)$ the centre of the dipole and $\delta$ the initial size of the perturbation.

The fringe region technique, extensively used and validated by Högberg & Henningson (1998), has been implemented for all simulations where the dynamics in a finite box, with the wake velocity profile imposed at the inlet of the box, $x = 0$, is of interest. It allows the efficient computation of the spatial evolution of the flow when perturbations are assumed to be zero at the inlet location. In a portion of the computational domain between the position we denote $x_{\text{sponge}}$ and $2L$ (typically in half the computation domain, i.e. $x_{\text{sponge}} = L$), a linear damping term $-A(x)w(x, y, t)$ is added to the evolution equation (2.1). The damping function $A(x)$ is smooth and given by the formula (Högberg & Henningson 1998)

$$
\left.
\begin{aligned}
&x < x_{\text{sponge}}: && A(x) = 0, \\[2mm]
&x_{\text{sponge}} < x < x_{\text{sponge}} + \delta_{\text{r}}: && A(x) = \frac{A}{1 + \exp\left(\dfrac{\delta_{\text{r}}}{x - x_{\text{sponge}}} + \dfrac{\delta_{\text{r}}}{x_{\text{sponge}} + \delta_{\text{r}} - x}\right)}, \\[4mm]
&x_{\text{sponge}} + \delta_{\text{r}} < x < 2L - \delta_{\text{f}}: && A(x) = A, \\[2mm]
&2L - \delta_{\text{f}} < x < 2L: && A(x) = \frac{A}{1 + \exp\left(\dfrac{\delta_{\text{f}}}{x - L + \delta_{\text{f}}} + \dfrac{\delta_{\text{f}}}{L - x}\right)}.
\end{aligned}
\right\} \tag{2.4}
$$

The damping intensity is determined by $A$, $\delta_{\text{r}}$ is the length of the region where the damping grows from zero to $A$, and $\delta_{\text{f}}$ the length of the region where the damping relaxes back to zero. In practice $\delta_{\text{r}}$ equals $L/2$ since it should be chosen large enough to avoid the backscattering of perturbations by the outlet condition, whereas $\delta_{\text{f}}$ should be short enough to have a small level of perturbations at the inlet and properly mimic the actual inlet condition. Values of $\delta_{\text{f}}$ between 1 and 10 spatial steps $\delta_x$ have been tested and none of the results presented are sensitive to this parameter. Furthermore, to ensure a proper vanishing of the perturbations in the sponge region and a level of perturbations at the inlet location $x = 0$ as close as possible to zero (i.e. of the order of the numerical precision of the Fourier transform: $10^{-13}$ for double precision

and $2 \times 10^5$ nodes) we have used a very strong damping coefficient $A$. The working value of $A$ is 10 in all simulations and should be compared to 0.5, the maximum growth rate of the instability. This high value, associated with a very fast drop of $A(x)$ at a few collocation points (usually 6 points), allows a proper simulation of the inlet condition where the amplitude of the perturbation should vanish. This fact, crucial when very precise second-order effects are to be analysed, has been carefully verified: the results are identical whether the damping coefficient is equal to 2 or to 50. Therefore the value of 10 for the damping coefficient has been chosen as adequate to enforce the inlet condition and optimal to save computation time, since a value of 50 requires a smaller time step to avoid numerical instabilities. It should be noted that this damping region or 'sponge' is very much larger and stronger, i.e. associated with a larger damping factor, than that used in boundary layers, which occupies only a tenth to a quarter of the domain with a smaller ratio of the damping factor to the instability growth rate. This is because we want to guarantee a fast evanescence of the perturbation upstream of the inlet.

As in Delbende & Chomaz (1998) the dynamics of the flow will be analysed using the enstrophy $\eta(x, t)$ computed at each streamwise location $x$ and time $t$ by

$$\eta(x, t) = \int_{-H/2}^{-H/2} \omega^2(x, y, t) \, \mathrm{d}y. \tag{2.5}$$

When the linear dynamics is of interest, a method relying on the demodulation of the wave packet is usually applied in order to compute the absolute and convective instability threshold with the highest precision for the shortest computational time. This method, extensively discussed in Delbende et al. (1998), has been used here to obtain the absolute growth rate presented in figure 2, but will not be recalled here since the goal of the paper is to describe strong nonlinear effects.

In most of the following, the Reynolds number $Re = \Delta U D / \nu$, based on the wake width $D = 2$ and wake velocity deficit $\Delta U = U_\infty - U_0 = 2$, is fixed at 20 (except if explicitly stated otherwise) and the velocity ratio $\Lambda$ is then used as a control parameter. We have verified that the results are similar for large Reynolds numbers (see §§3 and 4) but smaller resolutions and longer computation times are then required to capture the viscous effect. The value of 20 is a compromise and allows us to compute very precisely second-order effects in a reasonable time. In particular, very close to the transition value between absolute and convective instability, the dynamics exhibits extremely long transients that require, for the closest point presented here, $2.5 \times 10^6$ time steps and three weeks of integration on a four-processor SGI Origin 2000 computer! Integration so close to the threshold for higher Reynolds number would thus have been prohibitive. In the following the box width $H$ is generally fixed to 8.4 to be compared to the width of the wake $D = 2$. This moderate confinement slightly displaces the absolute/convective transition but, as shown by Delbende & Chomaz (1998), the dynamics are similar for all confinements. Since boxes used are very long in $x$, this value for the box width has been chosen as another compromise to save computation time. The three boxes used are

(i) box $B_1$ of size $102.4 \times 8.4$ of effective length $L_1 = 51.2$, with collocation points on a $1024 \times 84$ grid, a sponge over 512 points ($x_{\mathrm{sponge}} = 51.2$), a damping that rises over 250 points ($\delta_r = 25$) and falls over 10 points ($\delta_f = 1$) with a damping parameter $A = 10$;

(ii) box $B_2$ of effective length $L_2 = 102.4$, twice as long as the box $B_1$, of size $204.8 \times 8.4$ with collocation points on a $2048 \times 84$ grid with a sponge such that $x_{\mathrm{sponge}} = 102.4$, $\delta_r = 50$, $\delta_f = 1$, and $A = 10$;
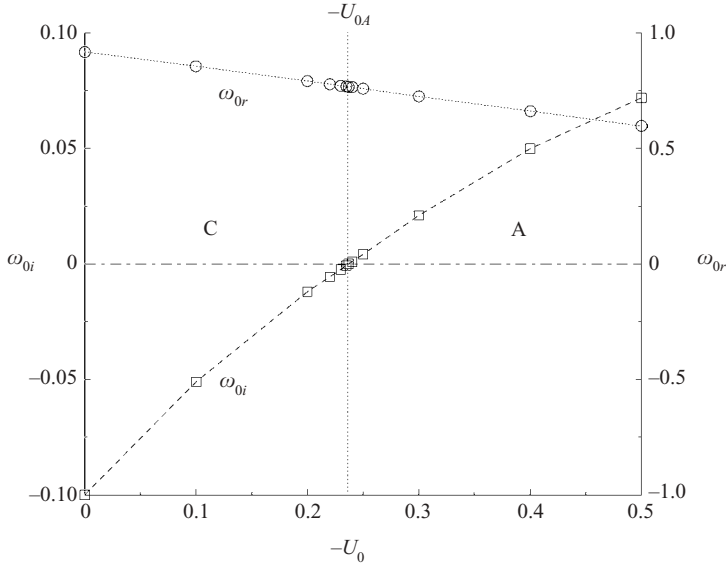
FIGURE 2. Absolute growth rate $\omega_{0i}$ and absolute frequency $\omega_{0r}$ as a function of $-U_0$ for $Re = 20$, deduced from the analysis of the linear wave packet in an 'unbounded' domain mimicked by the extremely long box $B_3$. When the absolute growth rate is positive ($\omega_{0i} > 0$) the flow is absolutely unstable (A), and it is convectively unstable (C) when $\omega_{0i} < 0$.

(iii) box $B_3$ of size $409.6 \times 8.4$ with collocation points on a $4096 \times 84$ grid and no sponge.

A fourth box $B_1'$ is used to test the confinement:

(iv) box $B_1'$ twice as wide as box $B_1$ (size $102.4 \times 16.8$ with collocation points on a $1024 \times 164$ grid) but identical otherwise.

## 3. Linear and nonlinear impulse responses

The linear and nonlinear impulse responses have been computed in box $B_3$ as a function of $U_0$ (or equivalently of $\Lambda$). The initial impulse of zero net circulation was given by equation (2.3). To test the ability of the sponge to 'absorb' perturbations without even a small reflection, the linear and nonlinear wave packets computed in the large box $B_3$ before the wave packet reaches the end of the domain have been compared to the same wave packet but computed in the smaller box $B_2$ with the sponge activated. Quite remarkably, the portion of the wave packet outside the sponge region was strictly identical in both simulations. Even the tail, whose amplitude, was more than ten decades smaller than the maximum amplitude, was properly computed in the small box. This result validates the sponge technique and proves that it does not induce non-local effects such as for example coupling between perturbations that leave the computational domain and the inlet boundary condition as observed by Buell & Huerre (1988) for the mixing layer.

Figure 2 presents the absolute growth rate $\omega_{0i}$, defined as the growth rate observed for large time, in the fixed reference frame, at the initial impulse perturbation location, as a function of $-U_0$, the velocity defect at the centre of the wake. When the growth rate $\omega_{0i}$ crosses zero, the instability becomes absolute. This defines a critical value for the transition to linear absolute instability $U_{0A} = -0.238 \pm 0.001$ or equivalently
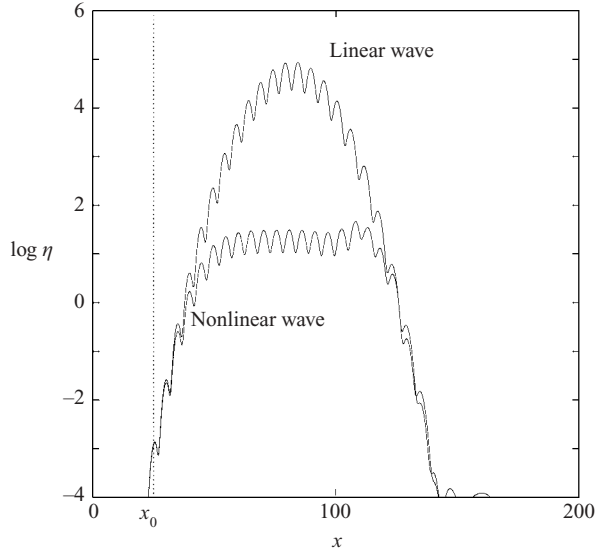
FIGURE 3. Comparison of the linear and nonlinear impulse response computed in the very long box $B_3$ for $Re = 20$ and $U_0 = U_{0A}$; the location of the initial impulse is shown by the vertical dotted line at $x_0$. The enstrophy of the linear and nonlinear wave packets at time $t = 100$ as a function of $x$ are plotted in as solid lines. Only less than half the computation domain is presented.

$\Lambda_A = -1.31$. Figure 2 also presents the absolute frequency $\omega_{0r}$ as a function of $-U_0$ for future reference.

To compare with the results by Monkewitz (1988), two other series of simulations were performed by varying the Reynolds number and keeping the velocity ratio constant with $\Lambda = -1$ ($U_0 = 0$, no flow in the wake) and $\Lambda = -0.909$ ($U_0 = 0.1$, a co-flow in the wake). Threshold values have been obtained and are in excellent agreement with the values given by Monkewitz (1988). For $\Lambda = -1$ the absolute instability occurs at $Re \sim 44.2$, the value reported by Monkewitz being 45.2, and for $\Lambda = -0.909$ we found a threshold at $Re \sim 125$, identical to the value estimated from Monkewitz's figure 2. As discussed in Delbende & Chomaz (1998), the confinement due to lateral boundaries may have very gently modified the absolute instability threshold but the comparison with Monkewitz indicates that this effect is negligible.

Figure 3 shows at time $t = 100$ the enstrophy of the linear wave packet as a function of $x$. This wave packet was initiated by an impulse dipole, given by equation (2.3) with $(x_0, y_0) = (23, 0.5)$, off the wake axis. Now, if the same numerical simulation is performed by inserting the nonlinearities into the Navier–Stokes equations, we simply obtain a gentle saturation of the exponentially growing part of the wave packet as shown in figure 3. This result, already discussed in Delbende & Chomaz (1998), is important since it shows that the front separating the saturated wake region from the unperturbed parallel wake flow moves at the speed of the edge of the linear wave packet. The fully nonlinear wake instability therefore follows the Dee & Langer (1983) scenario and is a pulled front. This result is not at all straightforward, since the theory of front propagation only prohibits fronts moving slower than the linear wave packet (see van Saarloos & Hohenberg 1992 for details) and the existence of fronts moving faster can only be excluded by a direct simulation such as that presented here or by analyses in phase space when simpler, one-dimensional, model evolution

equations are considered. Similar results have been obtained for Taylor–Couette and Rayleigh–Bénard instability by Büchel *et al.* (1996) and Müller *et al.* (1992) but the majority of instabilities in fluid mechanics have not yet been explored in this way.

## 4. Nonlinear global mode in a semi-infinite domain

The bifurcation of an open flow in a semi-infinite domain subject to an homogeneous inlet condition has been discussed in detail in Chomaz (1992), Couairon & Chomaz (1996, 1997*a*,*b*, 1999*b*) and Chomaz & Couairon (1999) using amplitude equations.

The predictions of the model are twofold. At leading order a self-sustained oscillation should occur when the front separating the unperturbed medium from a saturated state moves upstream. In the present case, since the previous section demonstrates that the front is linearly selected, a self-sustained global mode should exist when the linear instability becomes absolute, i.e. for $U_{0G}(Re) = U_{0A}(Re)$ or, if the Reynolds number is varied, for $Re_G(U_0) = Re_A(U_0)$. At threshold the selected global frequency is then the absolute frequency, $\omega_G = \omega_{0r}$, and the saturation occurs only at $x = \infty$. At second order, the analysis shows that when the threshold is exceeded, the distance at which the saturation occurs, the so-called healing length $\Delta_x$, varies inversely to the square root of the criticality with $\epsilon$, defined as the departure from threshold:

$$\Delta_x \propto \frac{1}{\sqrt{\epsilon}}. \tag{4.1}$$

When $U_0$ is varied and $Re$ is fixed, the departure from threshold is defined as $\epsilon = U_{0A}(Re) - U_0$, whereas when $Re$ is varied and $U_0$ is fixed, $\epsilon = Re - Re_A(U_0)$. As demonstrated in Couairon & Chomaz (1997*a*), this result describes well the behaviour of Rayleigh–Bénard convection when a throughflow is added, as reported by Müller *et al.* (1992) and of Taylor–Couette flow when a throughflow is added, as presented in Büchel *et al.* (1996).

I emphasize that if the front velocity were nonlinearly selected the bifurcation would occur while the flow is, at most, convectively unstable and the frequency selection and the scaling for the healing length would have been radically different as described in Couairon & Chomaz (1997*b*).

Figure 4 presents a time series of the spatially evolving vorticity field when the perturbations are forced to be zero at the inlet (indicated by the orange dots on the left of the first snapshot). In the case presented, the velocity ratio $\Lambda = -0.909$ and the flow at the inlet is everywhere positive ($U_0 = 0.1$ and $U_\infty = 2.1$). The Reynolds number is equal to 400 and is well above the absolute instability threshold ($Re_A = 125$) for this velocity ratio $\Lambda = -0.909$ ($U_0 = 0.1$). The roll-up of vortices is visible. The effect of the body force is in this case weak since the Reynolds number is high, but it still keeps the wake from diffusing before becoming unstable. The initial impulse perturbation induces a front of saturated vortices that first moves upstream and then stops at a certain distance from the inlet.

Similar direct numerical simulations of the wake when perturbations vanish at the inlet have been systematically performed for two cases: varying the Reynolds number and keeping the velocity ratio constant for $\Lambda = -1$ and, in a more intense manner, varying the velocity ratio and keeping the Reynolds number constant and equal to 20. In all the cases tested, no matter how the flow is initially perturbed (by a localized perturbation of small or order-unity amplitude, or by an initial white noise) the flow relaxes to zero when the instability is convective and takes the shape of a spatially
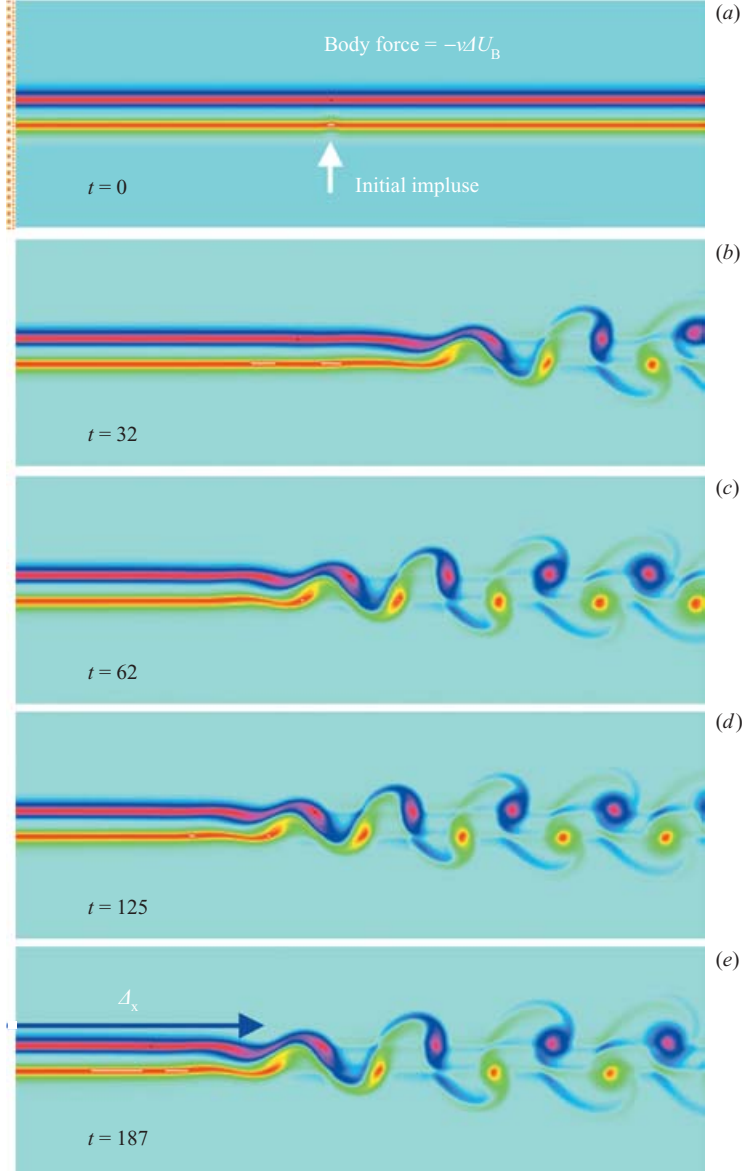
FIGURE 4. Global mode for $Re = 400$ and $\Lambda = -0.909$ ($U_0 = 0.1$, a co-flow in the wake) computed in box $B'_1$. Time series of the spatially evolving vorticity field when the perturbations are forced to be zero at the inlet (indicated by the orange dots on the left of the first snapshot). The domain shown is $51.2 \times 16.8$, the computational box being twice the length. (a) $t = 0$, (b) $t = 32$, (c) $t = 62$, (d) $t = 125$, (e) $t = 18.7$, The arrow in (e) shows $\Delta_x$.

growing instability that saturates at some distance from the inlet when the instability is absolute (figure 4).

Figure 5(a) shows the bifurcation diagram obtained for $Re = 20$ using computational boxes $B_1$ and $B_2$. The asymptotic amplitude is measured by the maximum vorticity of the nonlinear perturbation $\Omega_{max}$. At large time $\Omega_{max}$ is zero for all $-U_0$ smaller than $-U_{0A}$. When the absolute instability threshold is exceeded, i.e. for $-U_0 > -U_{0A}$, $\Omega_{max}$ rises extremely fast to a saturation value of order unity. The global
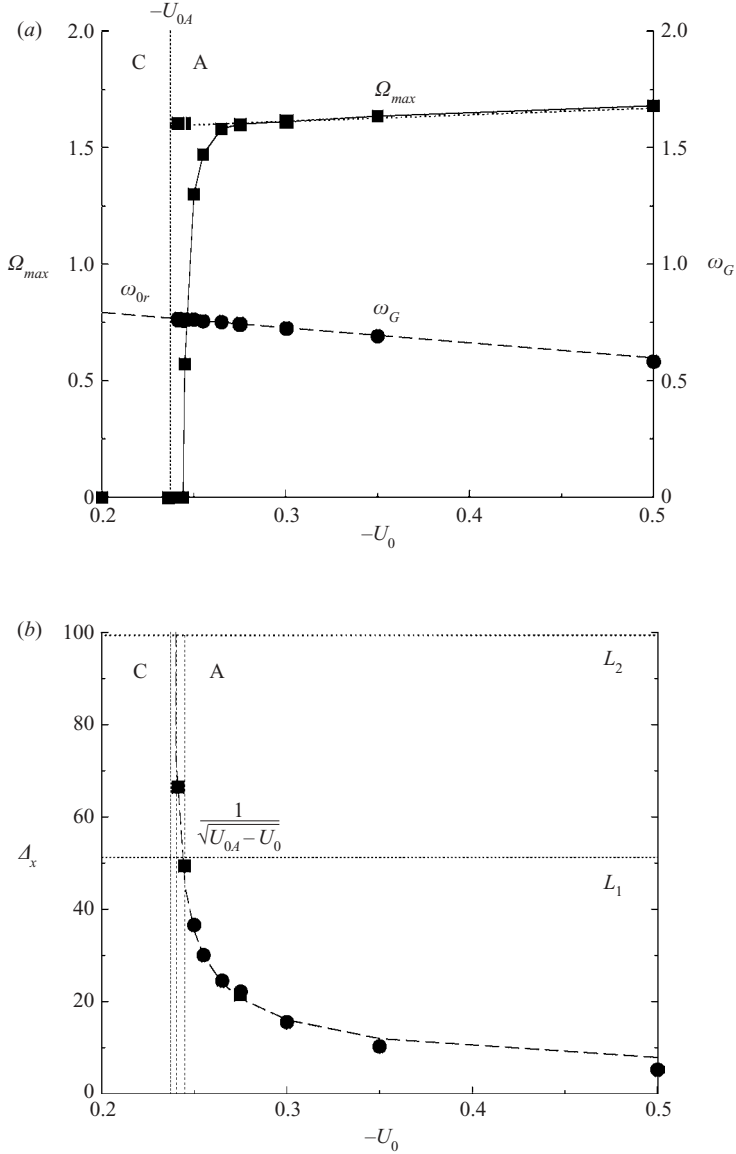
FIGURE 5. Global modes computed in box $B_1$. (*a*) Bifurcation diagram for $Re = 20$, showing the maximum vorticity (grey square symbols) of the nonlinear global mode $\Omega_{max} = \text{Max}_{xy}(\omega(x))$ as a function of $-U_0$, and the frequency of the global mode $\omega_G$ (grey circles); the dashed line represents the absolute frequency $\omega_{0r}$ already reported in figure 2. The global mode exists when the instability is absolute and its frequency equals the absolute frequency. Four extra points corresponding to computation in box $B_2$ are shown by black squares (for $\Omega_{max}$) and black circles (for $\omega_{0r}$) for $U_0 = -0.235$, $-0.24$, $-0.245$ and $-0.275$. (*b*) Healing lengths $\Delta_x$, the distance at which saturation occurs, as a function of $-U_0$ for global modes computed in box $B_1$. Three extra points corresponding to computation in box $B_2$ are shown by black squares for $U_0 = -0.24$, $-0.245$ and $-0.275$. No healing length is reported for $U_0$ smaller than $U_0A$ since no global modes exist below the absolute instability threshold.

frequency $\omega_G$ is equal the absolute frequency $\omega_{0r}$ for the whole range of $-U_0$ tested. At the absolute instability threshold this follows the theoretical prediction (Couairon & Chomaz 1997*a*).

For $0.24 < -U_0 < 0.255$ the amplitude seems not yet saturated when box $B_1$ is used. This is due to the finite streamwise size of the domain. For these values of $-U_0$ so close to $-U_{0A}$, local saturation is not reached at the end of the computational domain $B_1$. In fact for these cases, if the domain were infinite the saturation would have occurred at a healing distance larger than the length $L_1$ of the computational domain $B_1$. This streamwise confinement effect has been discussed in detail with respect to amplitude equations in Chomaz & Couairon (1999). This effect is confirmed by results of simulations in the double length box $B_2$ performed for $U_0 = -0.235, -0.24,$ $-0.245$ and $-0.275$. For $U_0 = -0.235$ the flow is stable and relaxes after a very large transient to zero. For the other values saturation is reached before the end of the domain $B_2$. For $U_0 = -0.275$ the maximum vorticity $\Omega_{max}$ and the healing lengths (to be precisely defined in the following) $\Delta_x$, plotted in figure 5(*b*), are identical for simulations in boxes $B_1$ and $B_2$. For $U_0 = -0.24$ and $-0.245$ the maximum vorticity $\Omega_{max}$ has reached saturation in the long box $B_2$ and its values are marked by a black square symbol in figure 5(*a*). As predicted in model equation studies, when the flow is parallel the bifurcation appears as a step and, in the long box $B_2$, the oscillation amplitude indeed jumps from zero at $U_0 = -0.235$ to a finite value at $U_0 = -0.240$. The healing lengths measured in box $B_2$ are marked by a black square symbol in figure 5(*b*) and are about the same size as in box $B_1$ or larger. Computations in box $B_1$ do not simulate an infinite domain when $-U_0$ is too close to $-U_{0A}$ (here, only for the two values $-0.24$ and $-0.245$) but the longer box $B_2$ does.

A similar bifurcation scenario is obtained by varying the Reynolds number and keeping the velocity ratio constant at $\Lambda = -1$. When the Reynolds number is above the threshold for absolute instability, $Re_A = 45$, a global mode appears and saturates closer to the inlet when $Re$ is increased. Numerical simulations in box $B_1$ show that the flow is stable for $Re = 40$, and unstable for $Re = 50$ with a healing length $\Delta_x = 24.5$. For $Re = 60, 80,$ and 120 the healing lengths are reduced respectively to $\Delta_x = 14.5, 10.5,$ and 7.5. The healing length verifies the theoretical scaling law (4.1) and varies approximately as $\Delta_x \sim 56/\sqrt{\epsilon} \sim 56/\sqrt{Re - Re_A}$.

The spatio-temporal diagrams in figure 6 compare the evolution of a large initial localized perturbation in a convectively unstable case $-U_0 < -U_{0A}$ and in an absolutely unstable case $-U_0 > -U_{0A}$. The early time evolution is similar in both cases: the generated wave packet rapidly spreads and grows. Then, as time goes on, the wave packet saturates. The speed $v_f$ of the trailing front is positive when the flow is convectively unstable (figure 6*a*) and negative when the flow is absolutely unstable (figure 6*b*). The front moves away from the inlet in the convective case (to the right on figure 6*a*) whereas it moves upstream when the flow is absolutely unstable (to the left on figure 6*b*) until it stops when it is blocked by the inlet. One may see in figures 6(*a*) and 6(*b*), that the evolution is very slow since the closer to the absolute threshold, the smaller the speed of the trailing front and the larger the time needed for the flow to adjust. Since the velocity of the front varies linearly with the criticality $\epsilon = U_{0A} - U_0$, the convergence time $T$ diverges as

$$T \propto \frac{L}{\epsilon}. \qquad (4.2)$$

This scaling law is verified well in the numerical simulations. I draw the attention of the reader to the very slow convergence process implied by equation (4.2), that requires 12500 dynamical time scales $U/L$ for the smaller criticality computed ($U_0 = -0.24$), i.e. $2.5 \times 10^6$ time steps representing 21 days of computation on a four-processor Origin 2000 SGI computer for the box $B_2$. Such a large CPU consumption was required
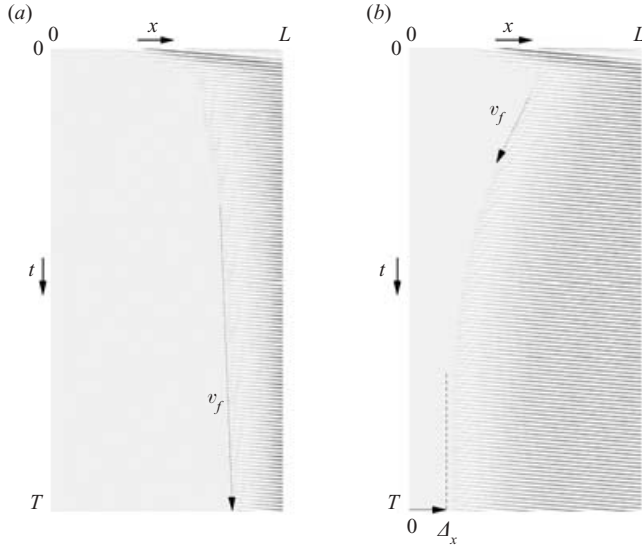
FIGURE 6. Spatio-temporal diagrams: (*a*) convectively unstable case $U_0 = -0.23$, (*b*) absolutely unstable case $U_0 = -0.275$. The domain size is 51.2 in $x$ and 750 in $t$.
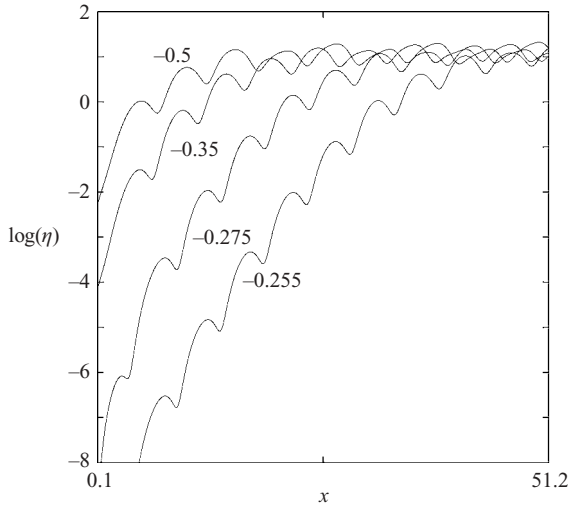


FIGURE 7. The enstrophy $\eta(x)$ as a function of $x$ for $-U_0 = 0.255, 0.275, 0.35$ and $0.5$.

in order to test convincingly the theoretically proposed scaling laws for the healing length $\Delta_x$ and the slope at the inlet $d\eta/dx$ reported in figure 8. This also explains why the global mode scaling laws have been extensively tested for a single Reynolds number $Re = 20$ whereas the cases with $\Lambda = -1$ and $\Lambda = -0.909$ have been explored in a more restricted manner.

The healing length $\Delta_x$ is defined as the distance at which the local enstrophy $\eta$ reaches the value unity as shown in figure 7, which displays the local enstrophy as a function of $x$ for four values of $U_0$. The smaller the departure from threshold the larger the distance at which saturation occurs. Once again, the physical idea that the dynamics of the global mode is governed by a front which would have
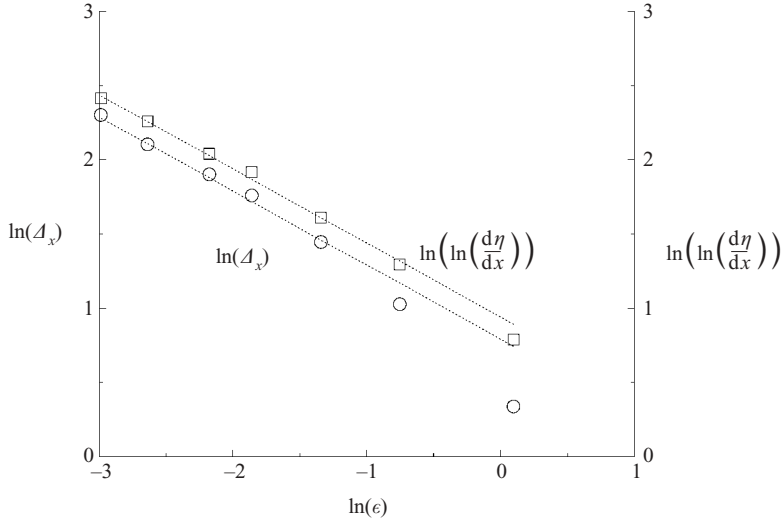
FIGURE 8. Healing length $\Delta_x$, and slope at the inlet $d\eta/dx$ as a function of the criticality $\epsilon = U_{0A} - U_0$ for $Re = 20$ as obtained in computational box $B_1$.

moved upstream if the inlet were not there, is clearly validated and the scaling law (4.1) proposed by the amplitude equation analysis is recovered well even far from the threshold. This scaling law may be physically understood by considering the beating of two spatial instability waves above the absolute instability threshold. At the absolute threshold $\epsilon = 0$ two spatial branches pinch (see for instance Huerre & Monkewitz 1990 for a definition of spatial branches). Above threshold the spatial waves corresponding to the real frequency of the saturated global mode $\omega_G$ have complex wavenumbers that differ by the square root of $\epsilon$ (since $\omega_G$ departs linearly in $\epsilon$ from the complex saddle node $\omega_0$). The two waves have opposite amplitudes at $x = 0$ in order for the perturbation to vanish at the inlet. Downstream, the wave with the largest growth rate will ultimately dominate. The difference between the spatial growth rates being of order $\sqrt{\epsilon}$, the distance at which one wave will dominate is therefore of the order $1/\sqrt{\epsilon}$.

The average slope at the origin of the local enstrophy plotted in figure 7, $d\eta/dx$, is drawn in figure 8. It should follow the scaling law (Couairon & Chomaz, 1997$a,b$)

$$\ln \frac{d\eta}{dx} \propto \frac{1}{\sqrt{\epsilon}}. \tag{4.3}$$

The agreement between the asymptotic scaling laws (4.1), (4.3) and the results from direct numerical simulation is excellent since it extends over two decades of $\epsilon$-variations. Once $\Delta_x$ predicted theoretically is smaller than the actual size of the computational domain, we see on figures 5($b$) and 8 that the measured value of $\Delta_x$ varies as if the domain were infinite. This confirms that the finiteness of the computational domain affects the flow only in a small vicinity of the bifurcation as already discussed for the bifurcation diagram (figure 5$a$).

As previously explained, the smallest value of $\epsilon$ for which converged values of $\Delta_x$ and $d\eta/dx$ may be obtained is limited by the length of the computational domain used and the convergence time $T$, which diverges at threshold. Indeed for smaller $\epsilon$ values, the use of the longer domain $B_2$ is required. The two extra values of $\Delta_x$ obtained in this case reported in figure 5($b$) are in excellent agreement with the
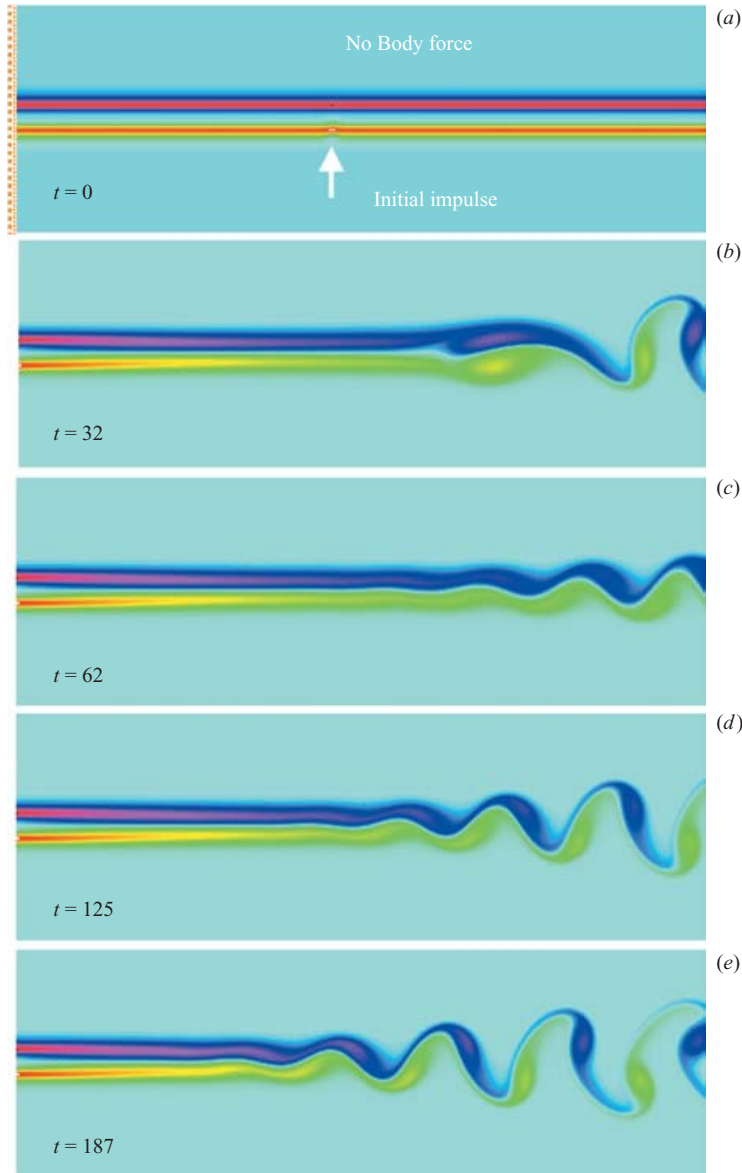
FIGURE 9. Global mode in a non-parallel flow for $Re = 800$ and $\Lambda = -0.909$ ($U_0 = 0.1$) computed in box $B_1'$. Time series of the spatially evolving vorticity field when the perturbations are forced to be zero at the inlet (indicated by the orange dots on the left of the first snapshot). The domain size is $51.2 \times 16.8$. (*a*) $t = 0$, (*b*) $t = 32$, (*c*) $t = 62$, (*d*) $t = 125$, (*e*) $t = 187$.

scaling law (4.1) plotted as a dashed line. Furthermore, in the parallel wake flows computed here, perturbations continue to be amplified to the end of the computation domain and for the longest box $B_2$ the total gain between the inlet and the outlet is already close to $10^{14}$. For longer boxes the gain is larger and the round-off error produces computational noise already sufficient to trigger noise-driven oscillations. This limitation is much less important for non-parallel flow since the gain does not increase indefinitely with the length of the computational domain. A similar effect is

well known in experiments (see Huerre & Monkewitz 1990 for a review) since the relative noise of wind tunnels and water channels is close to $10^{-4}$ and, when the spatial gain associated with a convective instability (or with a transient growth if the flow is stable) is larger than about $10^4$ noise-driven oscillations are observed (Cossu & Chomaz 1997). This is particularly the case for mixing layers or jets at large Reynolds numbers. When the instability is everywhere convective, noise-driven oscillations are observed whereas, in the absence of noise, the theory predicts a stable flow. When the counter-flow is increased in mixing layers or when the density of the jet is decreased, a pocket of absolute instability appears in the flow and a self-sustained mode replaces the noise-driven oscillations.

## 5. Conclusion

By adding a body force that compensates the diffusion of the basic flow and makes the flow parallel in the absence of perturbations, we have computed the dynamics of a wake flow directly generated at the inlet of the domain. We have established a link between the occurrence of a self-sustained oscillation (a global mode), and the linear and the nonlinear transition to absolute instability. First, as done by Delbende & Chomaz (1998), the nonlinearity associated with perturbations was shown to leave the propagation speed of the instability unchanged. More precisely we have shown that the front separating the saturated wake solution from the basic state propagates at the speed of the edge of the linear wave packet. The nonlinear absolute instability as defined by Chomaz (1992) coincides, therefore, with the linear absolute instability for this particular flow. Then, when a homogeneous inlet condition is applied at $x = 0$ (i.e. when the perturbations are assumed to vanish at $x = 0$) we have shown that the self-sustained oscillation, the nonlinear global mode, is triggered when the flow becomes absolutely unstable. The solution then includes a front blocked by the inlet condition, at a distance that decreases as the inverse of the square root of the criticality. The solution keeps some properties determined by the theory of linear instability although it is immediately fully nonlinear. In particular the global frequency is the absolute frequency.

For a real wake, no body forces are present and the basic flow that should be considered is non-parallel under the action of viscous diffusion. If the resulting non-parallelism is weak enough, the dynamics described here will prevail as soon as the healing length $\Delta_x$ is smaller than the length scale $\mathscr{L}$ of the variation of the basic flow. Couairon & Chomaz (1999$a$) have discussed this effect using an amplitude equation and were able to interpret the experimental results on wakes for trapezoidal and triangle cylinder bodies of Goujon-Durand, Jenffer & Wesfreid (1994), Zielinska & Wesfreid (1995) and Zielinska *et al.* (1997). In particular the scaling of the healing length $\Delta_x$ explains their result that the distance at which the maximum amplitude of the perturbation is reached varies as the square root of the criticality. Decreasing the body force slowly to zero should allow us to smoothly attain the realistic wake from a parallel flow and unambiguously separate the nonlinear effects described in the present contribution from non-parallel effects. This study is ongoing and will be reported in detail in a future publication. Here, results for only the non-parallel global mode obtained for $Re = 800$ and $\Lambda = -0.909$ ($U_0 = 0.1$) are displayed in figure 9. Initially the wake is parallel. At the same time the basic flow relaxes toward the non-parallel flow associated with the diffusion of the inlet velocity profile, and a self-sustained vortex street appears. This non-parallel global mode includes a front blocked by the inlet. The selected frequency is also the absolute frequency at the inlet if the flow were

parallel. Non-parallel effects have shifted the instability to higher Reynolds numbers and greatly altered the scaling laws for $\Delta_x$.

Pier & Huerre (2001) and Pier (2002) have described the dynamics of a wake when the absolute instability region is surrounded on both sides (upstream and downstream) by convective instability regions. In this case the global mode is associated with a front located at the position where its speed vanishes. Since the front speed for a wake is that of the pulled front, the front is located at the edge of the absolute instability domain. Numerical simulations (Pier & Huerre 2001) of a synthetic wake produced at the inlet as in the present paper, but decelerated by an adverse pressure gradient that promotes the absolute instability some distance downstream of the inlet, have clearly demonstrated the connection between the occurrence of global modes and front selection. Their results, holding for a separated absolute instability region, together with the present contribution where the absolute instability region is attached to the inlet, describe the two generic cases for the strongly nonlinear dynamics of self-sustained oscillations (nonlinear global modes) in open flows. Together, they extend to the nonlinear regime the analysis of Monkewitz *et al.* (1993) on the linear dynamics of open flows with an absolute instability region either attached to or detached from the inlet.

REFERENCES

AHLERS, G. & CANNEL, D. S. 1983 Vortex-front propagation in rotating Couette–Taylor flow. *Phys. Rev. Lett.* **50**, 1583–1586.

BEN-JACOB, E., BRAND, H., DEE, G., KRAMER, L. & LANGER, J. S. 1985 Pattern propagation in nonlinear dissipative systems. *Physica* D **14**, 348–364.

BILLANT, P., BRANCHER, P. & CHOMAZ, J. M. 1999 Three-dimensional stability of a vortex pair. *Phys. Fluids* **11**, 2069–2077.

BÜCHEL, P. B, LÜCKE, M., ROTH, D. & SCHMITZ, R. 1996 Pattern selection in the absolutely unstable regime as a nonlinear eigenvalue problem: Taylor vortices in axial flow. *Phys. Rev.* E **53**, 4764–4777.

BUELL, J. C. & HUERRE, P. 1988 Inflow/outflow boundary conditions and global dynamics of spatial mixing layers. In *Studying Turbulence Using Numerical Simulation Databases-II. Rep.* CTR-S88, pp. 19–27. NASA Ames/Stanford Center for Turbulence Research.

BUHLER, L. 1996 Instabilities in quasi-two-dimensional magnetohydrodynamic flows. *J. Fluid Mech.* **326**, 125–150.

CHOMAZ, J.-M. 1992 Absolute and convective instabilities in nonlinear systems. *Phys. Rev. Lett.* **69**, 1931–1934.

CHOMAZ, J.-M. & COUAIRON, A. 1999 Against the wind. *Phys. Fluids* **11**, 2977–2983.

CHOMAZ, J.-M. & COUAIRON, A. 2000 Propagating pattern selection and causality reconsidered. *Phys. Rev. Lett.* **84**, 1910–1913.

COSSU, C. & CHOMAZ, J.-M. 1997 Global measures of local convective Instability. *Phys. Rev. Lett.* **78**, 4387–4390.

COUAIRON, A. 1997 Modes globaux fortement non linéaires dans les écoulements ouverts. PhD Thesis, École Polytechnique.

COUAIRON, A. & CHOMAZ, J.-M. 1996 Global instabilities in fully nonlinear systems. *Phys. Rev. Lett.* **77**, 4015–4018.

COUAIRON, A. & CHOMAZ, J.-M. 1997*a* Absolute and convective instabilities, front velocities and global modes in nonlinear systems. *Physica* D **108**, 236–276.

COUAIRON, A. & CHOMAZ, J.-M. 1997b Pattern selection in the presence of a cross flow. *Phys. Rev. Lett.* **79**, 2666–2669.

COUAIRON, A. & CHOMAZ, J.-M. 1999a Fully nonlinear global modes in slowly varying flows. *Phys. Fluids* **11**, 3688–3703.

COUAIRON, A. & CHOMAZ, J.-M. 1999b Primary and secondary nonlinear global instability. *Physica* D **132**, 428456.

COUAIRON, A. & CHOMAZ, J.-M. 2001 Pushed global modes in weakly inhomogeneous subcritical flows. *Physica* D **158**, 129–150.

DEE, G. 1985 Dynamical properties of propagating front solutions of the amplitude equations. *Physica* D **15**, 295–304.

DEE, G. & LANGER, J. 1983 Propagating Pattern selection. *Phys. Rev. Lett.* **50**, 383–386.

DELBENDE, I. & CHOMAZ, J.-M. 1998 Nonlinear convective/absolute instabilities in parallel two-dimensional wakes. *Phys. Fluids* **10**, 2724–2736.

DELBENDE, I., CHOMAZ, J.-M. & HUERRE, P. 1998 Absolute and convective instabilities in the Batchelor vortex: a numerical study of the linear impulse response. *J. Fluid Mech.* **355**, 229–254.

DELFS, J., EHRHARD, J., MEIBURG, E. & ÖRTEL, H., JR. 1997 Lagrange identification of absolutely unstable regimes in wakes. *Acta Mech.* **122**, 89–97.

DRAZIN, P. G. & REID, W. H. 1981 *Hydrodynamic Stability*. Cambridge University Press.

FINEBERG, J. & STEINBERG, V. 1987 Vortex-front propagation in Rayleigh–Bénard convection. *Phys. Rev. Lett.* **58**, 1332–1335.

GOUJON-DURAND, S., JENFFER, P. & WESFREID, J. E. 1994 Downstream evolution of the Bénard-von Kármán instability, *Phys. Rev.* E **50**, 308–313.

HAMMOND, D. & REDEKOPP, L. 1997 Global dynamics of symmetric and asymmetric wakes. *J. Fluid Mech.* **331**, 231–260.

HARRIS, D., BASSOM, A. P. & SOWARD, A. M. 2000 An inhomogeneous Landau equation with application to spherical Couette flow in the narrow gap limite. *Physica* D **137**, 260–276.

HÖGBERG, M. & HENNINGSON, D. 1998 Secondary instability of cross-flow vortices in Falkner–Skan–Cooke boundary Layers. *J. Fluid Mech.* **368**, 339–357.

HUERRE, P. & MONKEWITZ, P. A. 1990 Local and global instabilities in spatially developing flows. *Annu. Rev. Fluid Mech.* **22**, 473–537.

KOLMOGOROV, A. N., PETROVSKY, I. G. & PISKUNOV, N. S. 1937 Investigation of a diffusion equation connected to the growth of materials, and application to a problem in biology. *Bull. Univ. Moscow, Ser. Int. Sec.* A **1**, 1–25.

KYLE, D. M. & SREENIVASAN, K. R. 1993 The instability and breakdown of a round variable-density jet. *J. Fluid Mech.* **249**, 619–664.

LINGWOOD, R. J. 1995 Absolute instability of the boundary layer on a rotating disk. *J. Fluid Mech.* **299**, 17–33.

LINGWOOD, R. J. 1996 An experimental study of absolute instability of the rotating-disk boundary-layer fow. *J. Fluid Mech.* **314**, 373–405.

MEUNIER, M., PROCTOR, M., SOKOLOFF, D., SOWARD, A. & TOBIAS, S. 1997 Asymptotic properties of a nonlinear $\alpha$-dynamo wave: period, amplitude and latitude dependence. *Geophys. Astrophys. Fluid Dyn.* **86**, 249–285.

MONKEWITZ, P. A. 1988 The absolute and convective nature of instability in two-dimensional wakes at low Reynolds numbers. *Phys. Fluids* **31**, 999–1006.

MONKEWITZ, P. A., BECHERT, D. W., BARSIKOW, B. & LEHMANN, B. 1990 Self-excited oscillations and mixing in a heated round jet. *J. Fluid Mech.* **213**, 611–639.

MONKEWITZ, P., HUERRE, P. & CHOMAZ, J. M. 1993 Global linear stability analysis of weakly non-parallel shear fows. *J. Fluid Mech.* **251**, 1–20.

MONKEWITZ, P. A. & NGUYEN, L. N. 1987 Absolute instability in the near-wake of two-dimensional bluff bodies. *J. Fluids Struct.* **1**, 165–184.

MÜLLER, H. W., LÜCKE, M. & KAMPS, M. 1989 Convective patterns in horizontal flow. *Europhys. Lett.* **10**, 451–454.

MÜLLER, H. W., LÜCKE, M. & KAMPS, M. 1992 Transversal convection patterns in horizontal shear flow. *Phys. Rev.* A **45**, 3714–3726.

PIER, B. 2002 On the frequency selection finite-amplitude vortex shedding in the cylinder wake. *J. Fluid Mech.* **458**, 407–417.

Pier, B. & Huerre, P. 2001 Nonlinear self-sustained structures and fronts in spatially developing wake fows. *J. Fluid Mech.* **435**, 145–174.

Pier, B., Huerre, P. & Chomaz, J.-M. 2001 Bifurcation to fully nonlinear synchronized structures in slowly varying media. *Physica* D **148**, 49–96.

Pier, B., Huerre, P., Chomaz, J.-M. & Couairon, A. 1998 Steep nonlinear global modes in spatially developing media. *Phys. Fluids* **10**, 2433–2435.

Powell, J. A., Newell, A. C. & Jones, C. K. R. T. 1991 Competition between generic and nongeneric fronts in envelope equations. *Phys. Rev.* A **44**, 3636–3652.

van Saarloos, W. 1987 Dynamical velocity selection: marginal stability. *Phys. Rev. Lett.* **58**, 2571–2574.

van Saarloos, W. 1988 Front propagation into unstable states: marginal stability as a dynamical mechanism for velocity selection. *Phys. Rev.* A **37**, 211–229.

van Saarloos, W. 1989 Front propagation into unstable states. ii. linear versus nonlinear marginal stability and rate of convergence. *Phys. Rev.* A **39**, 6367–6390.

van Saarloos, W. & Hohenberg, P. 1992 Fronts, pulses, sources and sinks in generalized complex Ginzburg-Landau equations. *Physica* D **56**, 303–367.

Soward, A. 2003 Thin aspect ratio $\alpha\omega$-dynamos in galactic discs and stellar shells. In *Advances in Nonlinear Dynamos* (ed. A. Feeriz-Mas & M. Nuñez), chap. 8. Taylor & Francis.

Sreenivasan, K. R., Raghu, S. & Kyle, D. 1989 Absolute instability in variable density round jets. *Exps. Fluids* **7**, 309–317.

Strykowski, P. & Niccum, D. 1991 The stability of countercurrent mixing layers in circular jets. *J. Fluid Mech.* **227**, 309–343.

Tobias, S. M., Proctor, M. R. E. & Knobloch, E. 1997 The role of absolute instability in the solar dynamo. *Astron. Astrophys.* **318**, 55–58.

Tobias, S. M., Proctor, M. R. E. & Knobloch, E. 1998 Convective and absolute instabilities of fluid flows in finite geometry. *Physica* D **113**, 43–72.

Triantafyllou, G. & Karniadakis, G. 1990 Computational reducibility of unsteady viscous fows. *Phys. Fluids* A **2**, 653–656.

Vincent, A. & Meneguzzi, M. 1991 The spatial structure and statistical properties of homogeneous turbulence. *J. Fluid Mech.* **225**, 1–20.

Woodley, B. & Peake, N. 1997 Global linear stability analysis of thin aerofoil wakes. *J. Fluid Mech.* **339**, 239–260.

Worledge, D., Knobloch, E., Tobias, S. M. & Proctor, M. R. E. 1997 Dynamo waves in semi-infinite and finite domains. *Proc. R. Soc. Lond.* A **453**, 119–143.

Yu, M.-H. & Monkewitz, P. A. 1993 Oscillations in the near field of a heated two-dimensional jet. *J. Fluid Mech.* **255**, 323–347.

Zielinska, B. J. A. & Wesfreid, J. E. 1995 On the spatial structure of global modes in wake flow. *Phys. Fluids* **7**, 1418–1424.

Zielinska, B. J. A., Goujon-Durant, S., Dusek, J. & Wesfreid, J. E. 1997 Strongly nonlinear effect in unstable wakes. *Phys. Rev. Lett.* **79**, 3893–3896.